Biomaterials 32 (2011) 7079–7085

Contents lists available at ScienceDirect

Biomaterials

journal homepage: www.elsevier.com/locate/biomaterials

A computational analysis of the insertion of carbon nanotubes into cellular membranes

Siegfried Höfinger [a,b,*], Manuel Melle-Franco [c], Tommaso Gallo [a], Andrea Cantelli [a], Matteo Calvaresi [a], José A.N.F. Gomes [c], Francesco Zerbetto [a]

[a] Dipartimento di Chimica "G. Ciamician", Università di Bologna, Via F. Selmi 2, 40126 Bologna, Italy
[b] Department of Physics, Michigan Technological University, 1400 Townsend Drive, 49931 Houghton, MI, USA
[c] Requimte, Departemento de Química e Bioquímica, Faculdade de Ciências, Universidade do Porto, Rua do Campo Alegre s/n, 4169-007 Porto, Portugal

ARTICLE INFO

Article history:
Received 14 April 2011
Accepted 7 June 2011
Available online 1 July 2011

Keywords:
Carbon nanotubes
Membrane insertion
Membrane mimicry
Dissipative particle dynamics

ABSTRACT

Carbon nanotubes have been proposed to serve as nano-vehicles to deliver genetic or therapeutic material into the interior of cells because of their capacity to cross the cell membrane. A detailed picture of the molecular mode of action of such a delivery is, however, difficult to obtain because of the concealing effects of the cell membrane. Here we report a systematic computational study of membrane insertion of individual carbon nanotubes and carbon nanotube bundles using two entirely different and unrelated techniques. First a static scan of the environmental free energy is carried out based on a membrane mimicry approach and different insertion geometries are assessed. Then the dynamics is investigated with a coarse-grained approach that was previously used in the study of the integration dynamics of nanoparticles into the bilayer. The results of both models point, for unfunctionalized carbon nanotubes, at a preference for the horizontal orientation inside the internal hydrophobic layer of the cell membrane. Finally, the energetics of the formation of bundles of carbon nanotubes is studied. The cellular membrane promotes aggregation of carbon nanotubes in its hydrophobic core and modifies the structural stability of the bundles.

1. Introduction

A large number of new ordered allotropes of carbon have been discovered and characterized in recent years: the most widely known are fullerenes, nanotubes and, recently, the long-thought impossible graphene [1,2]. The simplest carbon nanotube (CNT) is a single molecule made of a rolled-up section of a regular network of planar hexagons composed of carbon atoms. CNTs typically have extremely high aspect ratios with long axial lengths (up to millimeters) compared to just a few Ångströms in diameter. Apart from this structural peculiarity, CNTs also show a number of interesting properties; they are tough and robust materials with very high electric and thermal conductivity, and consequently, they have been proposed for a large number of novel technological applications ranging from materials science to nanomedicine.

CNTs are able to translocate across cellular membranes (the lipid bilayer), and this is the base of interesting devices like the nano-injector [3] and the unexpected fertilizer effect on tomato seeds [4]. Computer simulations have played a key role in studying the energetics and mechanics of how nanotubes and their spherical cousins, the fullerenes, may pierce through the lipid bilayer [5]. Lopez et al. argued that short hydrophobic tubes with hydrophylic termini would spontaneously insert into the bilayer [6]. The free energy of C_{60} insertion was calculated from molecular dynamics simulations that showed that the pristine C_{60}, being apolar, is spontaneously incorporated into the hydrophobic region of the bilayer [7]. Conversely, polar, functionalized, C_{60} was experimentally found to enter cells by clathrin mediated endocytosis [8]. Chemical functionalization of fullerene and nanotubes, a common practice to increase their solubility [9], also affects their toxicological profiles. For example, the lethal dose of functionalized C_{60} for human cells is by up to 7 orders of magnitude larger than that of pristine C_{60} [10]. The reasons for this are yet unclear but aggregation may play an important role [11]. Moreover, graphene and CNTs have been found to have different cytotoxic effects in neural cells [12]. A very recent computational study found the CNT mediated rupture of a phospholipid bilayer too costly a process to support

* Corresponding author. Dipartimento di Chimica "G. Ciamician", Università di Bologna, Via F. Selmi 2, 40126 Bologna, Italy. Tel.: +39 051 2099578; fax: +39 051 2099456.
E-mail addresses: shoefing@mtu.edu, siegfried.hoefinger@unibo.it (S. Höfinger).

0142-9612/$ – see front matter © 2011 Elsevier Ltd. All rights reserved.
doi:10.1016/j.biomaterials.2011.06.011

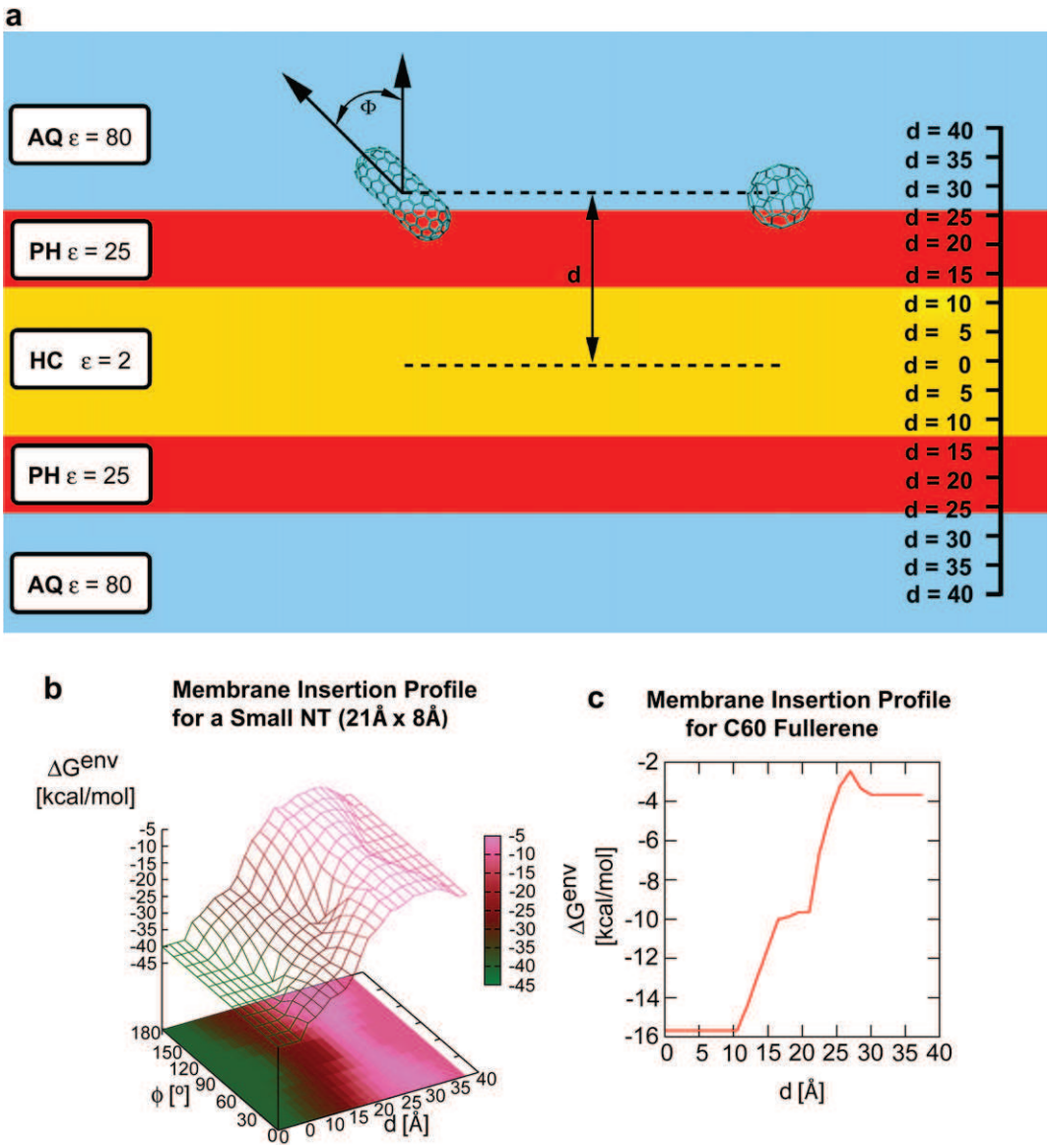

Fig. 1. Insertion of a small carbon nanotube (CNT) and C60 into the cell membrane. (a) Definition of the two variables ***d*** and ***Φ*** used for scanning the free energy landscape. In the membrane mimicry approach [21] three domains are taken into account, i.e., AQ (aqueous imitated by solvent water), PH (polar head group, 10 Å, simulated by solvent ethanol) and HC (hydrophobic core, 30 Å, simulated by solvent c-hexane). (b) Environmental free energy landscape for various CNT orientations as a function of ***d*** and ***Φ*** inside the lipid bilayer. (c) Free energy profile for the insertion of C60 into the cellular membrane.

direct spontaneous insertion of CNTs into cellular membranes [13]. Experimentally, pristine CNTs were found to severely damage the lipid bilayer in *E. coli* [14]. In contrast, DNA-functionalized, polar, CNTs were found to enter and leave the cell by endocytosis and exocytosis at comparable rates, explaining the low cytotoxicity of these materials [15].

Here we use different computational models to study the process of membrane insertion of CNTs and their bundles. The focus is on preferred geometric orientations and the basic dynamics underlying the insertion process. Only pristine materials are considered. A suggestion may be made for the toxicology of these carbon nanomaterials.

2. Materials and methods

2.1. CNT and C_{60} structures

The CNT used in this study is a (10,0) CNT closed by two hemi-C_{80} caps. The (10,0) CNT is a zig-zag, thin, semiconducting nanotube present to a certain degree in common nanotube samples [16]. Geometries of the (10,0) capped nanotubes and C_{60} were obtained from ab-initio calculations with the program Gaussian09 [17,18]. Bundle geometries were obtained with a computer program originally developed to investigate fullerenes in nanotubes and multishell nanotubes [19,20]: the Rigid Molecule Random Explorer (RMRE) algorithm randomly moves the molecules and minimizes the energy for a large number of configurations. 200 cycles of RMRE with a cutoff of 9 Å were used to locate the global minimum for each bundle.

2.2. Free energy calculations

Environmental free energies, ΔG^{env}, were computed according to the membrane mimicry approach [21] (AQ: aqueous domain modeled by water, PH: polar head group domain, 10 Å, modeled by ethanol, HC: hydrophobic core domain, 30 Å, modeled by cyclohexane). Membrane mimicry is itself inspired by the experimental measurements of Ashcroft et al. [22]. Corresponding molecular mechanics (MM) energies — when needed — were computed based on AMBER parameters [23]. Atom type CA was assigned to all atoms in C_{60} and CNTs, applying no partial charge (QM-derived ESP charges had shown negligible contributions on the order of 1 kcal/mol) and default van der Waals parameters of $r_{vdw} = 1.908$ Å and $\varepsilon_{vdw} = 0.086$ kcal/mol together with the scaling constants reported in ref. [21]. Both terms were combined to estimate free energies following MM/PBSA directives [24]. However, the PBSA term was replaced with ΔG^{env} as reported previously in ref. [25] leading to

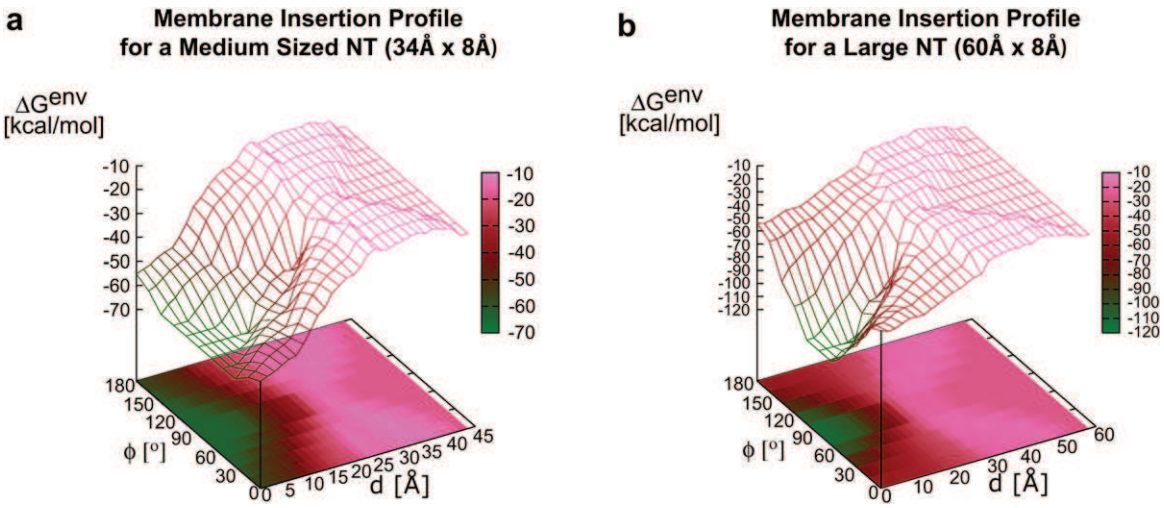

Fig. 2. Membrane insertion of a medium length and a longer length CNT. (a) The medium length CNT (34 Å × 8 Å) pathway shows features similar to the small CNT of Fig. 1b. (b) The longer length CNT (60 Å × 8 Å) exhibits increased preference for horizontal orientations ($\Phi \approx 90^{\circ}$) once it is inside the core domain of the cellular membrane.

$\Delta G^{MM/PB++}$ free energies. Surfaces were computed with program SIMS [26] but care has been taken to correct for internal cavities occasionally formed with small sized probe sphere radii. Membrane layers were defined relative to the CNT (always assumed to be centered at the origin and oriented along the *x*-axis). This is simply achieved by defining the midlayer of the cellular membrane via a specific normal vector and a central point. Individual atoms in the C_{60}/CNT-structures are then probed for their position within the cellular membrane and domain-specific parameters become assigned.

2.3. Dissipative particle dynamics

DPD calculations [27,28] were carried out with program CULGI 4.0.0 [29]. The simulation system was composed of water, lipids and a CNT. Lipids were represented by single chains of soft spheres and water by coarse-grained soft spheres. A single lipid unit was composed of three head beads (hydrophilic part) and twelve tail beads (hydrophobic part). DPD parameters were taken from the model of Shillcock and Lipowsky [30] capable of reproducing the structural properties and the stress profile of bilayers. CNTs were set up as colloidal particles of cylindrical shape. We follow the method described in ref. [31]. Specific methodological details are given in the Supplementary Information. DPD runs were repeated three times with largely identical outcome (for analysis and movie rendering a single run was chosen arbitrarily).

2.4. Advantages and limitations of the techniques employed

The major advantage with both computational techniques employed here is clearly the efficiency and ease with which atomic scale insight may be gained into rather complicated processes taking place in a rather complex environment. While the computation of environmental free energies, ΔG^{env}, should be regarded a static approach (every single pose of the CNT relative to the cellular membrane constitutes an individual problem, independent from all the rest), DPD is a dynamic approach [27,28], where we can study the time evolution of CNT insertion over long time scales. However, this efficiency comes at the prize of reduced accuracy and both methods are subject to characteristic technical limitations. The ΔG^{env} calculations follow a continuum approximation where the lipid bilayer is just divided into a reduced set of specific domains (see Fig. 1a), hence detailed local atomic interactions are not represented explicitly. Similarly, DPD does not resolve the involved molecular structure into atoms (both the CNT as well as the lipid bilayer), but rather

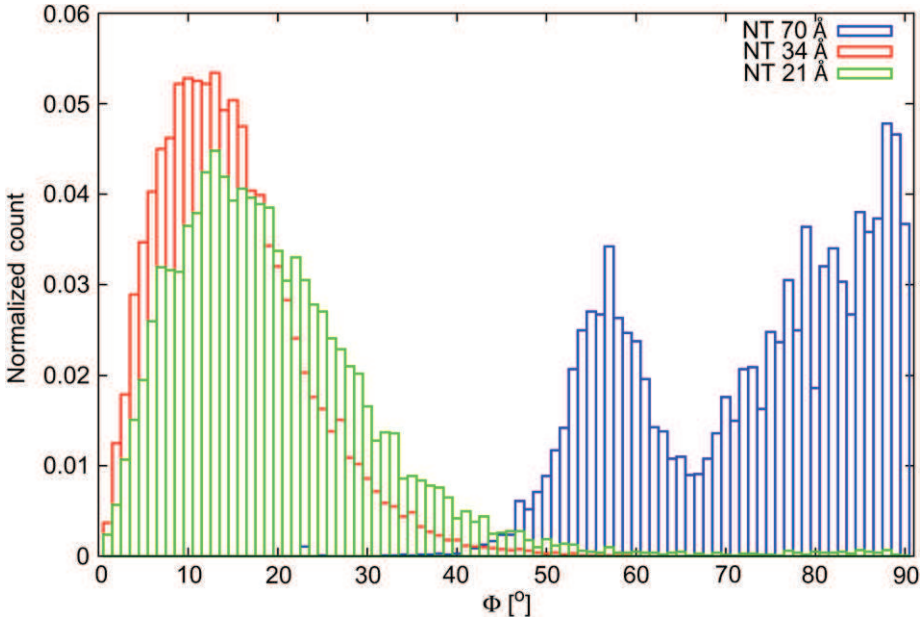

Fig. 3. Dissipative particle dynamics (DPD) simulations [27–29,32]. Distribution of angles, Φ, for different CNT lengths (21 Å, green, 34 Å, red and 70 Å, blue). The longer the CNT, the more likely horizontal orientations are established.

uses coarse-grained beads instead (a group of atoms forms a single bead and the interaction between beads is given from a reduced set of simple rules). Consequently, DPD calculations can be very useful to obtain a qualitative understanding of a certain process while ΔG^{env} considerations can provide a first semi-quantitative assessment of the energetics involved. Care must be taken with either approach and the availability of experimental data for the process under investigation increases the likelihood to apply such models in a constructive analytical way. With regard to error bounds, the conformational dynamics of molecular sizes comparable to the ones studied here accounts for ΔG^{env} variations on the order of $\pm$10 kcal/mol mainly due to ΔG^{pol} [21]. Because here all atomic partial charges are set to zero, the ΔG^{pol} term does not contribute. The major source of inaccuracy will therefore be the ΔG^{cav} term from which a $\pm$10 kcal/mol variation may still be regarded as a reasonable error estimate.

3. Results and discussion

A scan of the environmental free energy landscape was carried out for various orientations of a single carbon nanotube (CNT) that was gradually immersed into the cellular membrane. In addition to the CNT also C_{60} was used for comparison. The intent was to provide a basis for comparison with data published previously in ref. [7]. Evaluations are based on the membrane mimicry approach [21] that was recently validated experimentally [25]. We define two geometric variables, $\boldsymbol{d}$ and $\boldsymbol{\Phi}$, that identify the position with respect to the cellular membrane, $\boldsymbol{d}$ is the center-to-center distance between the CNT and the midplane of the cellular membrane, $\boldsymbol{\Phi}$ is the angle defined between the membrane normal and the axis of the CNT (see Fig. 1a). Angles, $\boldsymbol{\Phi}$, in the range [0°,180°] are probed with increments of 18° and distances, $\boldsymbol{d}$, between 0 Å and 37 Å were examined with increments of 1.5 Å.

Initially a short CNT, 21 Å × 8 Å, was studied. A total number of 250 different $\boldsymbol{d}$, $\boldsymbol{\Phi}$ combinations was examined and the results are summarized in Fig. 1b. The landscape describing the environmental free energy must be symmetric with respect to $\boldsymbol{\Phi} = 90°$, a property that can be used to monitor the internal consistency of the model. A CNT approaching from the outside aqueous domain, AQ, first gets into contact with the polar head group layer, PH, at $\boldsymbol{d} \approx 35$ Å. The subsequent movement toward the interior of the membrane produces, at $\boldsymbol{d} \approx 29$ Å, a small barrier of 3.5 kcal/mol (ΔG^{cav} slightly increased) which is minimal for $\boldsymbol{\Phi} \approx 90°$. Along the insertion coordinate, there is a subsequent local minimum at $\boldsymbol{d} \approx 20$ Å (ΔG^{cav} significantly decreased), and a final minimum when the CNT is fully immersed in the hydrophobic core domain, HC, at $\boldsymbol{d} \approx 11$ Å with ≈ -40 kcal/mol of stabilization energy resulting from membrane embedding. Despite the small variations, the free energy surface forms a funnel favoring $\boldsymbol{\Phi} \approx 90°$ that can pictorially be described as "orientational funnel". Once embedded into the HC, all $\boldsymbol{\Phi}$ angles become accessible to the CNT without any other type of environmental penalty. A short CNT should therefore be able to assume all possible orientations inside the HC domain.

Similarly, the free energy profile for the insertion of C_{60} (see Fig. 1c) exhibits a tiny barrier of $\approx$1 kcal/mol upon entry at

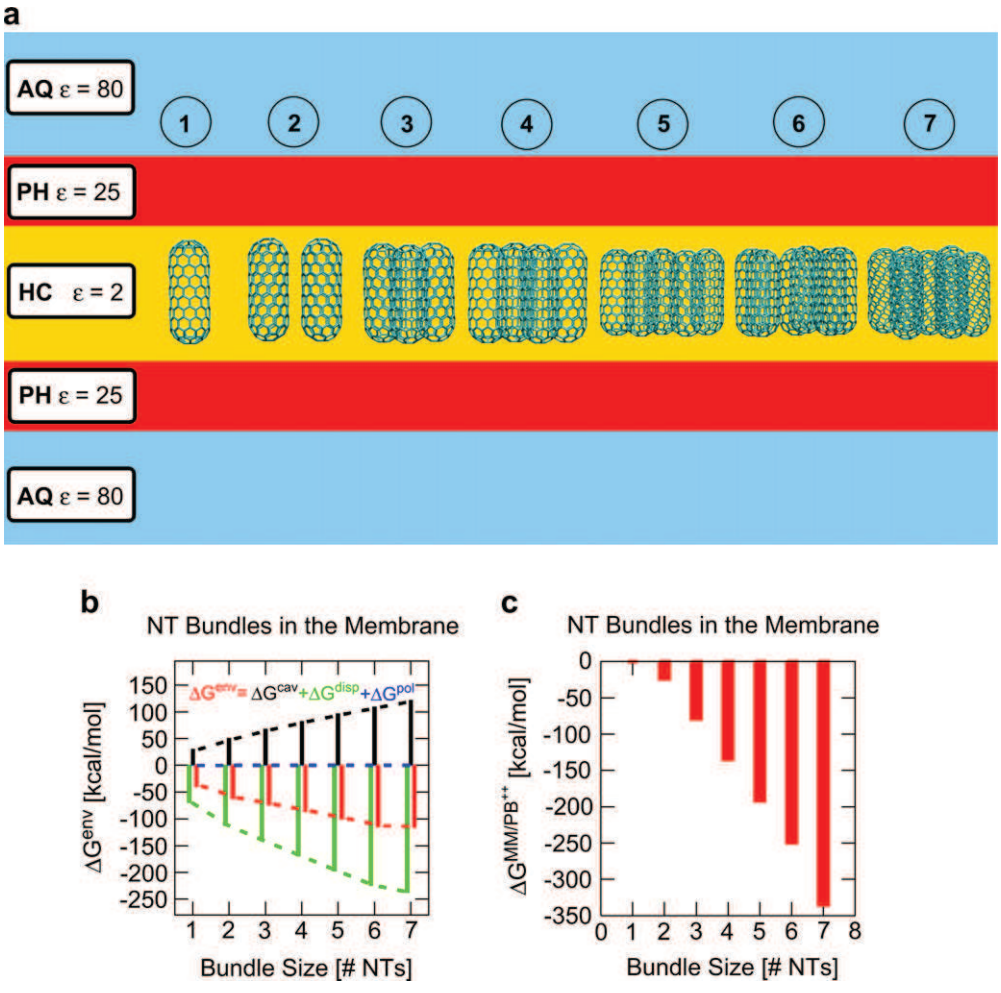

Fig. 4. Accumulation of small carbon nanotubes (CNTs) in the cellular membrane. The bundle size in terms of CNT units is given. (a) Schematic representation of the series of CNT bundles studied. (b) Environmental free energies and partial contributions for CNT bundles studied inside the cellular membrane. (c) Full association free energies ($\Delta G^{MM/PB++}$ [24,25]) for CNT bundles of increasing size.

$\boldsymbol{d} \approx 27$ Å, i.e., when the C_{60} has halfway penetrated into the PH domain. From this point, the penetration proceeds downhill on the free energy profile to an intermediate plateau at 15 Å $< \boldsymbol{d} <$ 20 Å of ≈ -10 kcal/mol environmental free energy when C_{60} is fully inside PH or at the interface between PH and HC. The thermodynamically preferred domain for C_{60} is the HC domain with a free energy gain comparable to that reported previously (compare the −20 kcal/mol by Bedrov et al. [7] to the −16 kcal/mol obtained here).

Next we turned our attention to the effect of an increased aspect ratio of the CNT. A medium length CNT (34 Å × 8 Å) and a longer CNT (60 Å × 8 Å) were subjected to the same procedure outlined above to scan the free energy landscape. Results are summarized in Fig. 2. Similar general characteristics of the environmental free energy surface are observed for both of the longer CNTs (compare Fig. 2a and b to Fig. 1b). The entry into the cellular membrane is marginally favored when the tube is flat on the surface. The global minimum is reached when the CNT is fully embedded in the lipid bilayer. However, when the medium length CNT is fully immersed in the HC domain ($\boldsymbol{d} \approx 0$ Å) the extreme angles are less favored than in Fig. 1b (see the green island in Fig. 2a delimited by $0° < \boldsymbol{\Phi} < 40°$ and $140° < \boldsymbol{\Phi} < 180°$). Accordingly, a medium length CNT prefers a slightly tilted orientation with both tips avoiding the PH domain. The longer length CNT (60 Å) further confirms this general picture, except that the overall stabilization free energy grows in magnitude and the window of preferred angles becomes narrower (see the shrunk green island in Fig. 2b, $60° < \boldsymbol{\Phi} < 120°$). Consequently, the general picture emerging from the membrane mimicry calculations is that with increasing CNT length there is a preference for horizontal embeddings in the core domain of the cellular membrane.

Application of a second — entirely different and unrelated — method was deemed necessary to complement the results. We performed simulations in the framework of Dissipative Particle Dynamics (DPD) [27,28,32] which had been shown to provide reasonable descriptions of the lipid bilayer. DPD is a coarse-grained model based on the "poor" and "good" interactions that are typically used to describe solvent–polymer interactions. The presence of hydrophilic and hydrophobic regions in the cellular membrane and the hydrophobicity of pristine CNTs makes the system ideal for this kind of treatment. DPD allows to follow the evolution in time of a chemical system of larger dimensions over longer time scales than purely atomistic simulations.

Three different CNTs were set up of 21 Å, 34 Å, and 70 Å in length and 10 Å in diameter. The chosen dimensions are comparable to those used in the membrane mimicry study. Results are best illustrated by

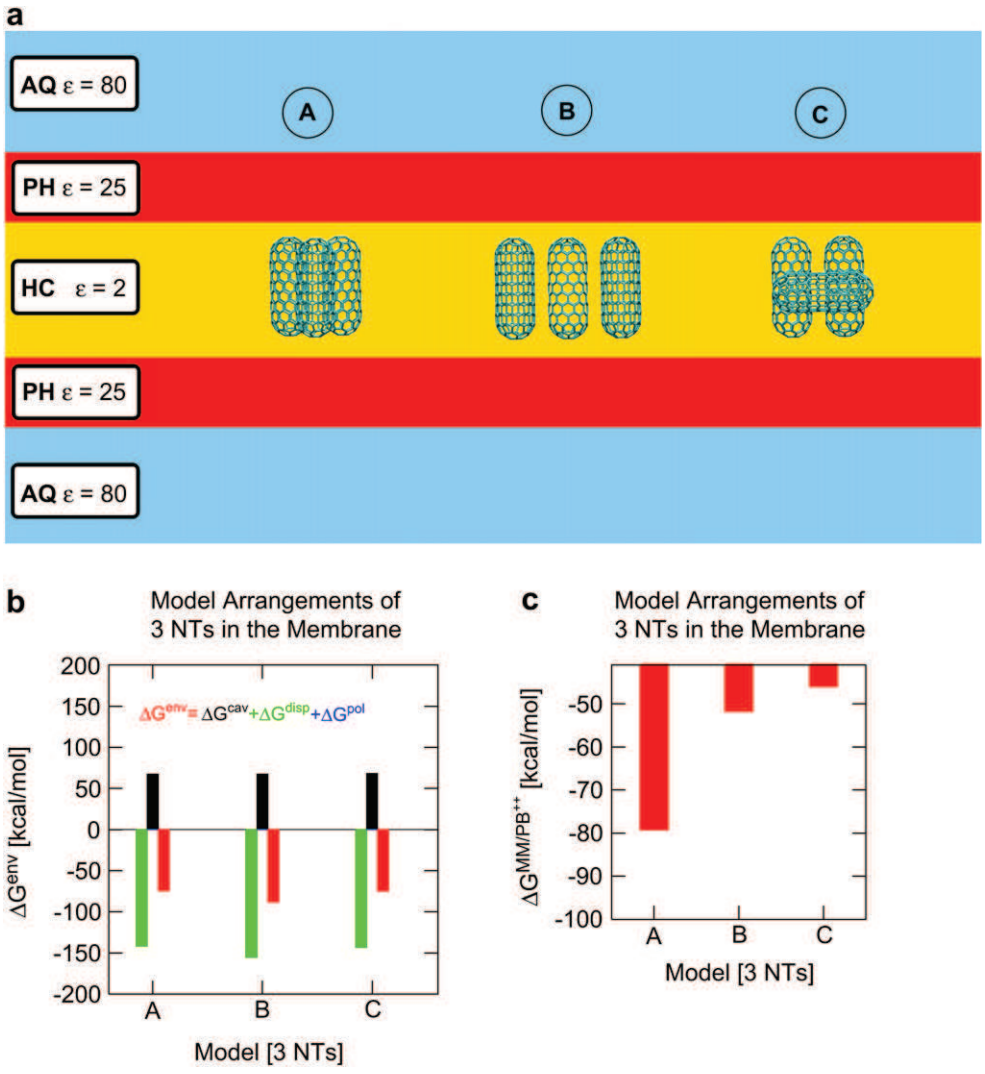

Fig. 5. Comparison of different geometric arrangements of 3 small carbon nanotubes (CNTs) in the cellular membrane. (a) Schematic representation of different model geometries examined for a group of 3 CNTs embedded in the lipid bilayer. (b) Environmental free energies and partial contributions for the 3 model geometries of 3 CNTs inside the lipid bilayer. (c) Full association free energies, $\Delta G^{MM/PB++}$.

the 3 movies available in the Supplementary Information (DPD_CNT21.mpg, DPD_CNT34.mpg and DPD_CNT70.mpg). Key results are also summarized in Fig. 3 and Supplementary Figs. 1–4. The DPD-time-averaged distributions of the characteristic angle, Φ, of Fig. 1a are shown in Fig. 3 for the three CNTs (21 Å in green, 34 Å in red and 70 Å in blue). Increasing the CNT length makes dominant the flat or horizontal orientations of the CNT with respect to the cellular membrane. Fig. 3 shows the shift in the angle distribution toward $\Phi \approx 90^\circ$ for the longest CNT. The relative positions of the CNT center with respect to the cellular membrane, as a function of DPD simulation time, are shown in Supplementary Fig. 1a. The initial short entrance stage is followed by an extended residence period inside the core domain of the cellular membrane. In practice, Supplementary Fig. 1a presents the process in which the CNT pierces through the lipid bilayer and accommodates itself in the hydrophobic core. Shorter CNTs show a kinetic preference for orientations parallel to the lipid tails. During the penetration, the Φ angle changes as shown in Supplementary Fig. 1b. It appears that the longest CNT prefers Φ angles close to $\Phi \approx 90^\circ$.

An important point can now be made: the DPD simulations as well as the environmental free energy scans suggest a preference of longer CNTs for horizontal embeddings in the core part of the cellular membrane (also consult movies DPD_CNT21.mpg, DPD_CNT34.mpg and DPD_CNT70.mpg and Supplementary Figs. 2–4).

The overall agreement of the two unrelated models can be used to explore further issues with the less computational intensive membrane mimicry model. One such issue is related to the finding that the degree and type of bundling has been found to affect CNT cytotoxicity [11]. A graphical representation of the systems investigated (bundles composed of up to 7 small CNTs) is given in Fig. 4a.

The CNTs selected to investigate the bundles are 10 Å in length and 8 Å in diameter. Individual groups of CNTs (bundles) were set up, optimized in vacuum by a global minimization procedure, placed in the cellular membrane and assessed for their environmental free energies. The parallel bundling of CNTs positioned perpendicular to the lipid bilayer allows a straightforward lateral extension to larger CNT assemblies. Fig. 4b summarizes environmental free energies, and their partial contributions, for CNT bundles inside the cellular membrane. Main contributions stem from dispersion (green) and cavitation (black) while polarization (blue) appears negligible. The trend of Fig. 4b shows that for the bundle with 7 CNTs the total environmental free energy (dashed red line) reaches a plateau, that is there is a saturation effect that is caused by the presence of the cellular membrane rather than by the bundling. This is an important feature that is amenable to experimental verification. However, full association free energies, $\Delta G^{MM/PB++}$ [25] do invert this trend (see Fig. 4c). The latter is a variant of MM/PBSA analysis [24] that accounts for environmental effects as well as direct interaction between complex-forming units, i.e., individual CNTs in this particular case (Δ refers to the same number of isolated CNTs). Here the additional MM-term is responsible for the consideration of the stabilization/de-stabilization resulting from inter-molecular interaction between adjacent CNT units (in the different geometric arrangements shown in Fig. 4a). MM-terms are completely absent in Figs. 1–3 because there we are looking only at a single object interacting with just the environment whereas with bundling also inter-CNT type of interaction comes into play. MM-terms are classically computed within the "molecular mechanics" approximation using the AMBER force [23]. Contrary to the environmental effect alone (see Fig. 4b) full association free energies do not show any tendency to level off. Consequently, self-assembly of large CNT bundles can be anticipated.

A final issue worth exploring is related to the effect of embedding different bundle arrangements in the cellular membrane. In order to investigate this aspect, we used a cluster of three CNTs in three different configurations, A, B, C shown in Fig. 5a. Configuration A is the global minimum in vacuum, while B and C are local minima. Environmental free energies and partial contributions for the three model geometries are given in Fig. 5b (dispersion, green, cavitation, black). Model geometry B is slightly favored by −13 kcal/mol over A and C (red bars) with dispersion being the decisive factor (compare trend of green/black bars to trend of red bars in Fig. 5b). However, in combining environmental effects as well as direct interactions, i.e., computing again $\Delta G^{MM/PB++}$ energies [24,25], model A is clearly the favored arrangement (see Fig. 5c where the reference state regarding the Δ is again a set of three isolated CNTs considered non-interacting in vacuum). Consequently, the model suggests the possibility of regular accumulation of parallel CNTs in the hydrophobic core domain of the lipid bilayer.

4. Conclusion

Two entirely unrelated techniques have been applied to study insertion of CNTs into the cellular membrane. The free energy surface describing the insertion process is very smooth. Horizontal conformations that place the CNT in the innermost hydrophobic layer of the cellular membrane are preferred by both approaches. The modeling also shows that short CNTs can be accumulated in the hydrophobic core domain of the cell membrane.

Acknowledgments

Funding by the University of Bologna is gratefully acknowledged. MMF acknowledges support by the Portuguese "Fundação para a Ciência e a Tecnologia" through the program Ciência 2008.

Appendix. Supplementary information

Supplementary data associated with this article can be found in the online version, at doi:10.1016/j.biomaterials.2011.06.011.

Three movies showing DPD simulations of CNTs of varying length integrating into the cellular membrane (DPD_CNT21.mpg, DPD_CNT34.mpg and DPD_CNT70.mpg). Five figures showing time-resolved DPD data and selected movie frames. Two sections with details on DPD unit conversion and employed DPD parameters.

References

[1] Geim A. Nobel lecture, random walk to graphene. Available from: http://nobelprize.org/nobel_prizes/physics/laureates/2010/geim-lecture.html; 2010.
[2] Novoselov K. Nobel lecture, graphene: materials in the flatland. Available from: http://nobelprize.org/nobel_prizes/physics/laureates/2010/novoselov-lecture.html; 2010.
[3] Chen X, Kis A, Zettl A, Bertozzi CR. A cell nanoinjector based on carbon nanotubes. Proc Natl Acad Sci U S A 2007;104:8218–22.
[4] Khodakovskaya M, Dervishi E, Mahmood M, Xu Y, Li Z, Watanabe F, et al. Carbon nanotubes are able to penetrate plant seed coat and dramatically affect seed germination and plant growth. ACS Nano 2009;3:3221–7.
[5] Yang K, Ma YQ. Computer simulation of the translocation of nanoparticles with different shapes across a lipid bilayer. Nat Nanotechnol 2010;5:579–83.
[6] Lopez CF, Nielsen SO, Moore PB, Klein ML. Understanding nature's design for a nanosyringe. Proc Natl Acad Sci U S A 2004;101:4431–4.
[7] Bedrov D, Smith GD, Devande H, Li L. Passive transport of C60 fullerenes through a lipid membrane: a molecular dynamics simulation study. J Phys Chem B 2008;112:2078–84.
[8] Li W, Chen C, Ye C, Wei T, Zhao Y, Lao F, et al. The translocation of fullerenic nanoparticles into lysosome via the pathway of clathrin mediated endocytosis. Nanotechnology 2008;19:145102.
[9] Georgakilas V. Supramolecular chemistry and self-assembly special feature: supramolecular self-assembled fullerene nanostructures. Proc Natl Acad Sci U S A 2002;99:5075–80.
[10] Sayes CM, Fortner JD, Guo W, Lyon D, Boyd AM, Ausman KD, et al. The differential cytotoxicity of water soluble fullerenes. Nano Lett 2004;4:1881–7.

[11] Wick P, Manser P, Limbach LK, Dettlaff-Weglikowska U, Krumeich F, Roth S, et al. The degree and kind of agglomeration affect carbon nanotube cytotoxicity. Toxicol Lett 2007;168:121–31.
[12] Zhang Y, Ali SF, Dervishi E, Xu Y, Li Z, Casciano D, et al. Cytotoxicity effects of graphene and single-wall carbon nanotubes in neural phaeochromocytoma-derived PC12 cells. ACS Nano 2010;4:3181–6.
[13] Pogodin S, Baulin VA. Can a carbon nanotube pierce through a phospholipid bilayer? ACS Nano 2010;4:5293–300.
[14] Kang S, Pinault M, Pfefferle LD, Elimelech M. Single wall carbon nanotubes exhibit strong antimicrobial activity. Langmuir 2007;23:8670–3.
[15] Jin H, Heller DA, Sharma R, Strano MS. Size dependent cellular uptake and expulsion of single-walled carbon nanotubes: single particle tracking and a generic uptake model for nanoparticles. ACS Nano 2009;3:149–58.
[16] Paolucci D, Melle-Franco M, Iurlo M, Marcaccio M, Prato M, Zerbetto F, et al. Singling out the electrochemistry of individual single-walled carbon nanotubes in solution. J Am Chem Soc 2008;130:7393–9.
[17] Frisch MJ, Trucks GW, Schlegel HB, Scuseria GE, Robb MA, Cheeseman JR, et al. Gaussian 09, revision A.1. Wallingford, CT: Gaussian, Inc.; 2009.
[18] Pfeiffer R, Kramberger C, Peterlik H, Kuzmany H, Kräutler B, Melle-Franco M, et al. FT-Raman characterization of the antipodal bis-adduct of C60 and anthracene. Phys Status Solidi B 2009;246:2794–7.
[19] Bellarosa L, Bakalis E, Melle-Franco M, Zerbetto F. Interactions in concentric carbon nanotubes: the radius vs the chirality angle contributions. Nano Lett 2006;6:1950–4.
[20] Chamberlain TW, Pfeiffer R, Peterlik H, Kuzmany H, Zerbetto F, Melle-Franco M, et al. Polyarene-functionalized fullerenes in carbon nanotubes: towards controlled geometry of molecular chains. Small 2008;4:2262–70.
[21] Kar P, Seel M, Weidemann T, Höfinger S. Theoretical mimicry of biomembranes. FEBS Lett 2009;583:1909–15.
[22] Ashcroft R, Coster HG, Smith J. The molecular organisation of bimolecular lipid membranes. The dielectric structure of the hydrophilic/hydrophobic interface. BBA-Biomembranes 1981;643:191–204.
[23] Case DA, Cheatham III TE, Darden T, Gohlke H, Luo R, Merz Jr KD, et al. The AMBER biomolecular simulation programs. J Comput Chem 2005;26:1668–88.
[24] Wang J, Morin P, Wang W, Kollman PA. Use of MM-PBSA in reproducing the binding free energies to HIV-1 RT of TIBO derivatives and predicting the binding mode to HIV-1 RT of Efavirenz by docking and MM-PBSA. J Am Chem Soc 2001;123:5221–30.
[25] Worch R, Bökel C, Höfinger S, Schwille P, Weidemann T. Focus on composition and interaction potential of single-pass transmembrane domains. Proteomics 2010;10:4196–208.
[26] Vorobjev YN, Hermans J. SIMS: computation of a smooth invariant molecular surface. Biophys J 1997;73:722–32.
[27] Hoogerbrugge PJ, Koelman JMVA. Simulating microscopic hydrodynamic phenomena with dissipative particle dynamics. Europhys Lett 1992;19:155–60.
[28] Groot RD, Warren PB. Dissipative particle dynamics: bridging the gap between atomistic and mesoscopic simulation. J Chem Phys 1997;107:4423–35.
[29] Culgi BV. The Netherlands. Available from: http://www.culgi.com; 2011.
[30] Shillcock JC, Lipowsky R. Equilibrium structure and lateral stress distribution of amphiphilic bilayers from dissipative particle dynamics simulations. J Chem Phys 2002;117:5048–61.
[31] Calvaresi M, Dallavalle M, Zerbetto F. Wrapping nanotubes with micelles, hemimicelles, and cylindrical micelles. Small 2009;5:2191–8.
[32] Reynwar BJ, Illya G, Harmandaris VA, Müller MM, Kremer K, Deserno M. Aggregation and vesiculation of membrane proteins by curvature-mediated interactions. Nature 2007;447:461–4.